Environmental Science & Technology

pubs.acs.org/est

Article

Gas-to-Aerosol Phase Partitioning of Atmospheric Water-Soluble Organic Compounds at a Rural Site in China: An Enhancing Effect of NH_3 on SOA Formation

Shaojun Lv, Fanglin Wang, Can Wu, Yubao Chen, Shijie Liu, Si Zhang, Dapeng Li, Wei Du, Fan Zhang, Hongli Wang, Cheng Huang, Qingyan Fu, Yusen Duan, and Gehui Wang*

Cite This: *Environ. Sci. Technol.* 2022, 56, 3915−3924

Read Online

ACCESS | Metrics & More | Article Recommendations | Supporting Information

ABSTRACT: Partitioning gaseous water-soluble organic compounds (WSOC) to the aerosol phase is a major formation pathway of atmospheric secondary organic aerosols (SOA). However, the fundamental mechanism of the WSOC-partitioning process remains elusive. By simultaneous measurements of both gas-phase WSOC (WSOCg) and aerosol-phase WSOC (WSOCp) and formic and acetic acids at a rural site in the Yangtze River Delta (YRD) region of China during winter 2019, we showed that WSOCg during the campaign dominantly partitioned to the organic phase in the dry period (relative humidity (RH) < 80%) but to aerosol liquid water (ALW) in the humid period (RH > 80%), suggesting two distinct SOA formation processes in the region. In the dry period, temperature was the driving factor for the uptake of WSOCg. In contrast, in the humid period, the factors controlling WSOCg absorption were ALW content and pH, both of which were significantly elevated by NH_3 through the formation of NH_4NO_3 and neutralization with organic acids. Additionally, we found that the relative abundances of WSOCp and NH_4NO_3 showed a strong linear correlation throughout China with a spatial distribution consistent with that of NH_3, further indicating a key role of NH_3 in WSOCp formation at a national scale. Since WSOCp constitutes the major part of SOA, such a promoting effect of NH_3 on SOA production by elevating ALW formation and WSOCg partitioning suggests that emission control of NH_3 is necessary for mitigating haze pollution, especially SOA, in China.

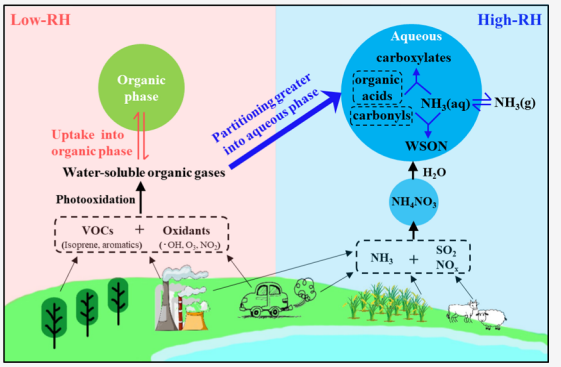

KEYWORDS: *ammonia uptake, aerosol liquid water (ALW), WSOC partitioning, brown carbon, aqueous-phase reaction*

1. INTRODUCTION

Water-soluble organic compounds (WSOC) abundantly exist in the atmosphere as gases and particulate matter and play an important role in atmospheric aqueous reactions and cloud condensation nuclei (CCN) formation due to their affinity with water, imposing significant impacts on global and regional climate change.[1,2] In addition, WSOC can affect human health because some of them are toxic.[3] WSOC can be directly emitted from sources or secondarily produced from the photooxidation of both gaseous and particulate organic matter (OM).[4−7] The gas-phase photooxidation of volatile organic compounds (VOCs) followed by partitioning to the condensed phase is the major formation pathway of atmospheric secondary organic aerosols (SOA).[8,9] Such a gas-to-condensed phase conversion process is complex, and the relevant mechanisms remain elusive due to the complexity of their chemical compositions and the subsequent aqueous reactions; the latter can significantly change the Henry's law constant of WSOC, leading to large model underestimations on SOA loadings.[9−11]

To date, only a limited number of field measurements have been conducted to understand the WSOC-partitioning mechanisms. Results have shown that the gas-to-particle phase partitioning of WSOC is dependent on many factors, such as meteorological parameters, gaseous species compositions, and condensed phase properties. For instance, Hennigan et al. investigated the gas- and aerosol-phase WSOC distribution in Atlanta, and found that the production of SOA in the city during summer was dominated by the partitioning of semivolatile gases to atmospheric water, which was affected by relative humidity (RH) and NO_x but had no visible relation to temperature and O_3 levels.[12] Recently, results based on observations in the United States suggested that high NH_3 concentrations could promote oxalic acid partitioning by

Received: October 11, 2021
Revised: March 4, 2022
Accepted: March 8, 2022
Published: March 17, 2022

https://doi.org/10.1021/acs.est.1c06855
Environ. Sci. Technol. 2022, 56, 3915−3924

enhancing the particle pH but were not significant for other small organic acids.[13] In recent years, a shift from sulfate-dominated to nitrate-dominated atmospheric $PM_{2.5}$ has been reported in China due to the strict control on SO_2 emissions.[14] Since NH_4NO_3 has a lower deliquescent point than $(NH_4)_2SO_4$, the increasing relative abundance of NH_4NO_3 in the current atmosphere over China makes the airborne particles more hygroscopic than before and thus facilitates the formation of aerosol liquid water (ALW), especially in winter haze periods.[15,16] ALW is the major fraction of airborne aerosols, which can serve as a medium for aqueous reactions and promote the formation of secondary aerosols.[17] Recently, a model study pointed out that the inorganic/water-rich phase plays a critical role in the formation of organic aerosols, as the availability of an absorptive medium is a key factor for the partitioning of WSOC.[18] A few studies on aerosol acidity indicated that the pH of $PM_{2.5}$ in China is approximately 2 units higher than that in the United States due to the much stronger emissions of NH_3 from both agricultural and nonagricultural sources.[14,19,20] Such increases in ALW content (ALWC) and differences in aerosol acidity between China and other countries may cause the gas-to-particle partitioning behavior of atmospheric WSOC in China to be different from that in other countries.

Several field studies have characterized the partitioning of individual water-soluble organic compounds in China.[10,21,22] For example, six carbonyls in the gas and particle phases were simultaneously measured in Beijing,[10] and the results showed that the particle-phase carbonyl concentrations were underestimated by a factor of $>10^3$ compared with the predictions from Henry's law. A study of gaseous and particulate formic acid in Shanghai showed that the partitioning of formic acid correlated well with ALWC in summer but not in winter.[21] Since the above compounds only account for a very minor fraction of the total WSOC mass in the atmosphere, the partitioning behavior of the six carbonyls and formic acid is not sufficiently representative for elucidating WSOC conversion. Therefore, bulk analysis of WSOC is necessary to improve our understanding of organic aerosol behavior in the Chinese atmosphere, especially in severe winter haze periods. In the current work, intensive field measurements of both gaseous and particulate species, including NH_3, organic acids, and WSOC, were performed at a rural site near Shanghai, China, during winter 2019, and the factors affecting the gas-to-particle phase-partitioning process were investigated. Our work revealed a crucial role of NH_3 in the gas-to-particle partitioning of WSOC and SOA formation in the country.

2. EXPERIMENTS

2.1. Observation Site Description. The observation site was located on the campus of the Yangtze River Delta (YRD) Estuary Wetland Station (31°44′N, 121°13′E) of East China Normal University (Figure S1), which is situated on western Chongming Island, a downwind region of the YRD urban agglomeration. Chongming Island is a rural area near Shanghai with no significant pollution sources around the observation site. The sampling inlet was located on a roof with a height of 6 m above the ground.

2.2. Measurements of the Gas- and Aerosol-Phase Species. Continuous measurements of inorganic ions, NH_3, WSOC, formic acid, acetic acid, and oxalic acid in the gas and aerosol phases and meteorological parameters were simultaneously conducted on Chongming Island from the 2nd of December 2019 to the 15th of January 2020. The above compounds were measured by an online system named IGAC (in situ gas and aerosol composition monitor; model 63GA, Fortelice International Co., Ltd., Taiwan, China), which was coupled with ICS-5000$^+$ ion chromatography (Thermo) and a TOC/TON analyzer (model TOC/TON-L CPH, Shimadzu, Inc., Japan). Due to the difference in the online instrument detection limits, gas-phase WSOC (WSOCg) and particle-phase WSOC (WSOCp) and particle-phase water-soluble organic nitrogen (WSON) were measured with a time resolution of 3 h, while other species were measured hourly. In this study, the concentrations of WSON were calculated as the difference between total nitrogen (TN), which was determined by the online TOC/TON analyzer, and total inorganic nitrogen (IN = $NH_4^+ + NO_2^- + NO_3^-$), which was determined by the IGAC-IC, namely, [WSON] = [TN] − [IN].[23]

To fully understand the WSOCp formation mechanism, the optical absorption of WSOCp at wavelengths of 300−550 nm was also measured using a UV−visible spectrophotometer (AOE Instrument, China). The detailed method for the optical measurement was reported by Wu et al.[24] $PM_{2.5}$ aerosols were also collected onto a precombusted (450 °C for 6 h) quartz fiber filter on a day/night basis using a high-volume air sampler (1.13 m^3 min^{-1}, TISCH) to analyze the filter-based WSOCp. To eliminate possible background interference, a HEPA filter was installed before and after the observation. The background level of the IGAC system accounted for less than 5.2% of the WSOC in the samples and was corrected for the reported data here. As shown in Figure S2, gaseous acetic acid and WSOCp determined by the IGAC system accounted for 73 and 89% of those measured in parallel by the PTR-MS and $PM_{2.5}$ filter-based analysis, respectively, demonstrating a good collection efficiency of the IGAC system. Details of the instrument application and method accuracy tests are documented in the Supporting Information (SI).

Three anions (SO_4^{2-}, NO_3^-, and Cl^-), five cations (Na^+, NH_4^+, K^+, Ca^{2+}, and Mg^{2+}) and three organic acids (formic, acetic, and oxalic acids) were measured in this study.[14,25] Simultaneous online monitoring of NH_3 and $PM_{2.5}$ was carried out during the study period. NH_3 was measured by a standard commercial CRDS spectrometer (model Picarro G2103, Picarro, Inc.) with a time resolution of 1 s. The detailed instrumentation was provided by He et al.[26] $PM_{2.5}$ was measured by an E-BAM continuous ambient $PM_{2.5}$ monitor. The organic carbon (OC) and elemental carbon (EC) of the $PM_{2.5}$ filter samples were analyzed by a DRI model 2001 thermal-optical carbon analyzer.[27] Meteorological parameters, including temperature and RH, were monitored by an automatic weather station (MILOS520, Vaisala, Inc., Finland), which was fixed on the roof of the observation station.

2.3. Calculations on ALWC and Acidity of $PM_{2.5}$. The thermodynamic model ISORROPIA-II was used to estimate the ALWC and acidity (pH) of $PM_{2.5}$ based on the hourly data of aerosol compositions (Na^+, NH_4^+, K^+, Ca^{2+}, Mg^{2+}, SO_4^{2-}, NO_3^-, and Cl^-), NH_3, and meteorological parameters (temperature and RH).[28] The forward metastable mode was chosen for the estimation since it is less sensitive to measurement errors than the reverse mode.[29] The data corresponding to an RH above 95% were excluded in this study because high RH could lead to large ALWC and pH estimation uncertainties.[30] The contributions of organic compounds to ALWC ($ALWC_{org}$) were calculated by

https://doi.org/10.1021/acs.est.1c06855
Environ. Sci. Technol. 2022, 56, 3915−3924

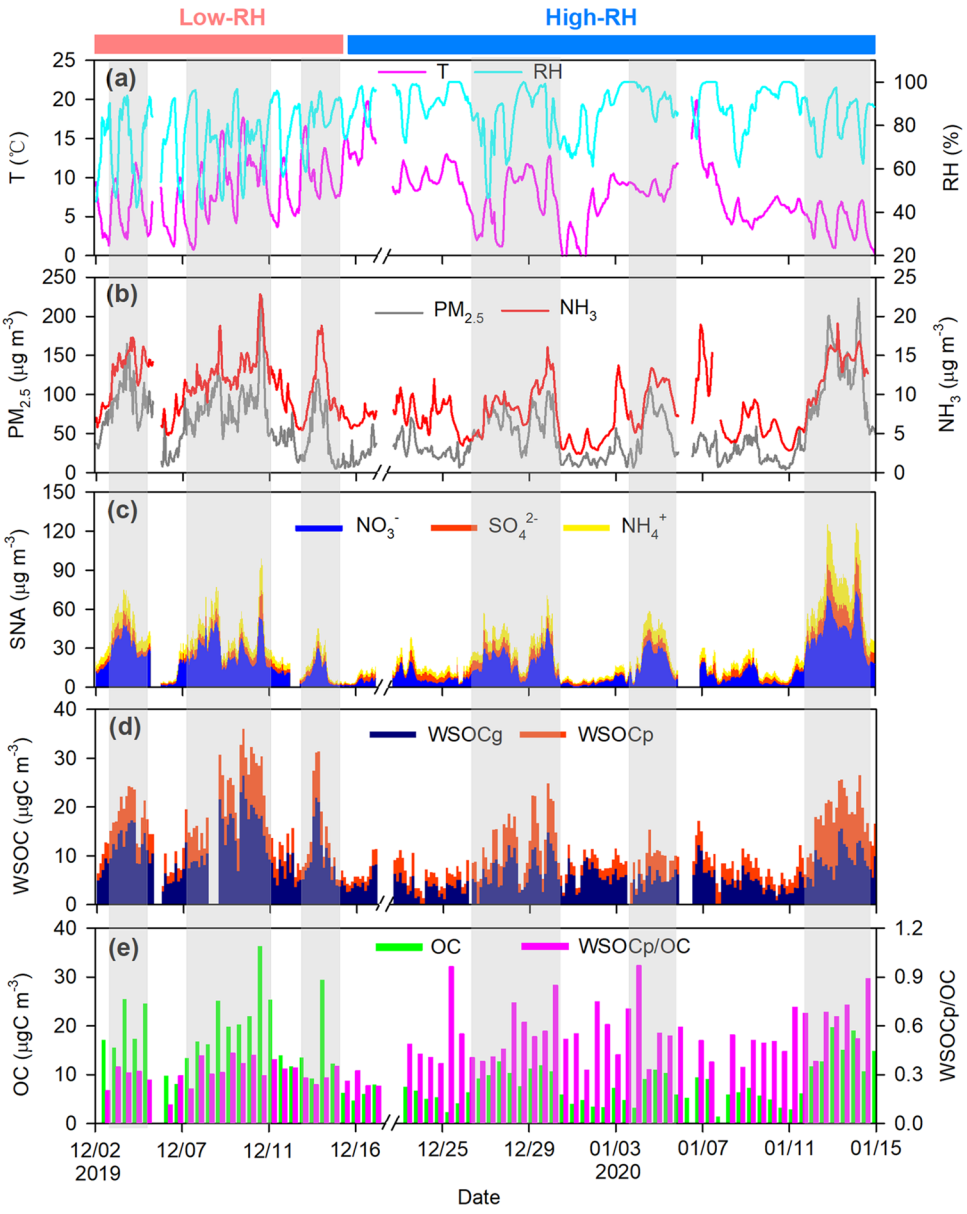

Figure 1. Temporal variations in major pollutants at the YRD background site on Chongming Island, China, during winter 2019. (a) RH and temperature, (b) $PM_{2.5}$ and NH_3, (c) total concentration of SNA (sulfate, nitrate, and ammonium), (d) the sum of gas- and aerosol-phase WSOC (WSOC = WSOCg + WSOCp), and (e) OC and the mass ratio of WSOCp to OC in $PM_{2.5}$ (the gray shadows indicate haze episodes with a daily $PM_{2.5}$ larger than 75 $\mu g\ m^{-3}$).

accounting for the mass concentration of OM. The calculation details are given in the Supporting Information.

3. RESULTS AND DISCUSSION

3.1. Chemical Characteristics of $PM_{2.5}$ Pollution during the Campaign. Temporal variations in meteorological parameters, major gaseous pollutants, and $PM_{2.5}$ compositions during the whole campaign and their statistical summary are shown in Figure 1 and Table 1, respectively. $PM_{2.5}$ on Chongming Island during the campaign was 55 ± 40 $\mu g\ m^{-3}$, with a daily concentration frequently exceeding the National Air Quality I Grade Standard of 35 $\mu g\ m^{-3}$, suggesting that fine particle pollution is still severe in China, especially in winter. As seen from Figure 1b, $PM_{2.5}$ showed a temporal variation similar to that of NH_3, indicating a possible linkage between NH_3 and $PM_{2.5}$ formation. NH_3 during the campaign was 9.3 ± 4.0 $\mu g\ m^{-3}$ with a maximum larger than 20 $\mu g\ m^{-3}$ (Table 1 and Figure 1b), which was approximately 10 times higher than that in a rural area in the southeastern United States,[31,32] suggesting severe NH_3 pollution in the YRD region. During the campaign, sulfate, nitrate, and ammonium (SNA) accounted for, on average, 10.9 ± 6.4, 25.7 ± 10.2, and 13.1 ± 4.4% of the $PM_{2.5}$ mass, respectively (Figure 1c). The carbonaceous species on Chongming Island during the campaign contributed to 30.7 ± 11.7% of the $PM_{2.5}$ and were dominated by OC (11.0 ± 7.1 $\mu gC\ m^{-3}$, Table 1). These results clearly demonstrated that nitrate and OC are the most abundant components of $PM_{2.5}$ in the YRD region. As shown in Table 1, WSOCg (7.4 ± 4.6 $\mu gC\ m^{-3}$) was approximately 50% higher than WSOCp (4.6 ± 2.9 $\mu gC\ m^{-3}$) on Chongming Island, indicating that WSOC in the YRD region mostly remains in the gas phase. Figure 1d shows that the temporal

https://doi.org/10.1021/acs.est.1c06855
Environ. Sci. Technol. 2022, 56, 3915−3924

Table 1. Concentrations ($\mu g\ m^{-3}$) of Major Pollutants and Meteorological Parameters in Chongming Island, China during Winter 2019

		low-RH (<80%)		high-RH (>80%)	
specie	average	clean	haze	clean	haze
$PM_{2.5}$	54.8 ± 40.5	19.5 ± 7.4	82.0 ± 32.2	24.1 ± 13.1	86.8 ± 39.1
OC	11.0 ± 7.1	8.3 ± 1.5	19.8 ± 6.6	5.1 ± 1.7	11.3 ± 3.5
WSOCg	7.4 ± 4.6	5.5 ± 1.6	12.1 ± 5.3	4.7 ± 2.2	7.7 ± 3.2
WSOCp	4.6 ± 2.9	2.4 ± 0.8	6.1 ± 2.6	2.6 ± 1.1	7.0 ± 3.1
WSON	1.9 ± 1.8	0.61 ± 0.56	2.3 ± 1.6	1.0 ± 1.3	3.7 ± 1.9
HCOOH(g)	1.5 ± 1.3	1.2 ± 0.61	2.7 ± 1.7	0.77 ± 0.06	1.3 ± 0.73
CH_3COOH(g)	3.0 ± 3.2	2.5 ± 1.2	6.1 ± 4.0	1.2 ± 0.41	2.8 ± 1.8
HCOOH(p)	0.13 ± 0.11	0.05 ± 0.03	0.22 ± 0.12	0.04 ± 0.02	0.22 ± 0.08
CH_3COOH(p)	0.13 ± 0.09	0.06 ± 0.03	0.19 ± 0.10	0.08 ± 0.02	0.20 ± 0.09
HOOCCOOH(p)	0.16 ± 0.08	0.09 ± 0.03	0.20 ± 0.08	0.10 ± 0.03	0.22 ± 0.07
Fp	0.38 ± 0.11	0.30 ± 0.07	0.34 ± 0.06	0.37 ± 0.10	0.47 ± 0.08
NO_3^-	16.1 ± 14.5	2.7 ± 2.1	23.6 ± 11.0	5.3 ± 4.2	29.1 ± 14.5
SO_4^{2-}	6.0 ± 4.1	2.4 ± 0.8	6.6 ± 2.8	3.6 ± 1.8	10.0 ± 5.0
NH_4^+	7.0 ± 5.5	1.6 ± 0.9	8.7 ± 3.7	3.3 ± 1.8	12.3 ± 6.2
NH_3	9.3 ± 4.0	6.9 ± 1.5	12.7 ± 3.0	6.3 ± 2.3	11.2 ± 3.3
O_3	45.7 ± 25.7	51.4 ± 15.5	36.9 ± 28.8	48.4 ± 20.8	51.4 ± 26.9
NO_2	22.6 ± 20.2	15.5 ± 13.9	40.1 ± 27.5	13.0 ± 10.4	22.2 ± 12.7
RH (%)	83.5 ± 13.6	77.0 ± 11.7	74.1 ± 15.4	89.0 ± 10.3	84.8 ± 11.4
T (°C)	7.8 ± 3.9	7.5 ± 4.6	8.1 ± 3.9	8.1 ± 3.8	6.3 ± 3.3

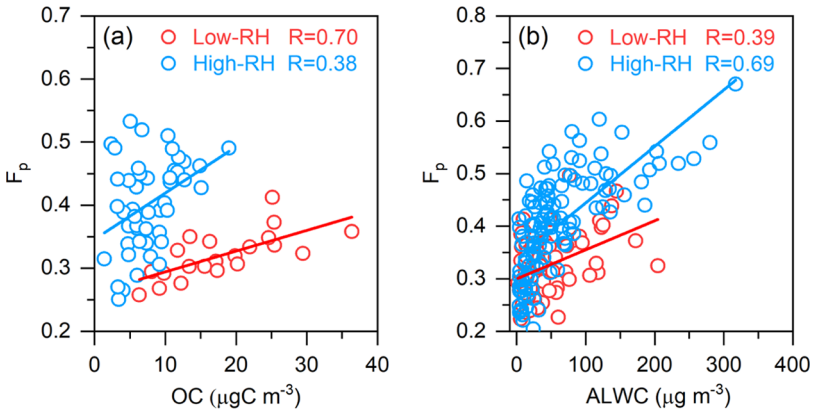

Figure 2. Linear regression analysis for Fp with (a) OC and (b) ALWC during the sampling periods under the low-RH (<80%) and high-RH (>80%) conditions. (Data in (a) are the values averaged on a day/night basis corresponding to the 12-h $PM_{2.5}$ filter samples.).

variation in WSOCp was similar to that of $PM_{2.5}$, with a strong correlation (R = 0.88) between WSOCp and $PM_{2.5}$, implying an important role of WSOCp in the haze formation process in the region.

As shown in Figure 1e, OC concentrations from 2nd to 14th December (17.8 ± 7.4 $\mu gC\ m^{-3}$) were much higher than those of the later periods, i.e., from 15th December 2019 to 15th January 2020 (8.1 ± 4.4 $\mu gC\ m^{-3}$). We also noticed a significant difference in relative humidity (RH) between these two periods (Figure 1a). Hence, the campaign was classified into a low-RH period (average RH <80%) from 2nd to 14th December and a high-RH period (average RH >80%) from 15th December 2019 to 15th January 2020. Such an 80% RH threshold is equal to the maximal deliquescence point of SNA and consistent with the findings by Renbaum-Wolff et al.,[33] who reported that ambient organic aerosols are liquid when RH is higher than 80%. Several haze episodes (with a daily $PM_{2.5}$ >75 $\mu g\ m^{-3}$) also occurred in both periods (gray shadows in Figure 1). Concentrations of NH_3 during the haze episodes in both periods were very close (Table 1), but the concentrations of SNA in the haze events were higher during the high-RH period than during the low-RH period (51.3 ± 25.1 versus 39.0 ± 17.0 $\mu g\ m^{-3}$, respectively, Table 1). Moreover, the haze level of WSOCg was 12.1 ± 5.3 $\mu gC\ m^{-3}$ during the low-RH period, which was approximately 60% higher than that (7.7 ± 3.2 $\mu gC\ m^{-3}$) in the high-RH period. However, the haze levels of WSOCp were almost equal between the relatively dry and humid periods (6.1 ± 2.6 versus 7.0 ± 3.1 $\mu gC\ m^{-3}$, respectively, Table 1), possibly due to a stronger gas-to-particle partitioning in the humid period. Since most WSOC in the atmosphere is secondarily produced, these results suggest that the gas-to-particle conversion of WSOCg has a great impact on SOA formation in the YRD region and probably evolves with different dynamic processes under dry and humid conditions.

3.2. Partitioning of WSOC into the Organic Phase in the Low-RH Period. To investigate the partitioning behavior of the WSOC, we calculated its partitioning coefficient (Fp = WSOCp/(WSOCp + WSOCg)) under different RH conditions, which was defined as the fraction of total WSOC in the

https://doi.org/10.1021/acs.est.1c06855
Environ. Sci. Technol. 2022, 56, 3915−3924

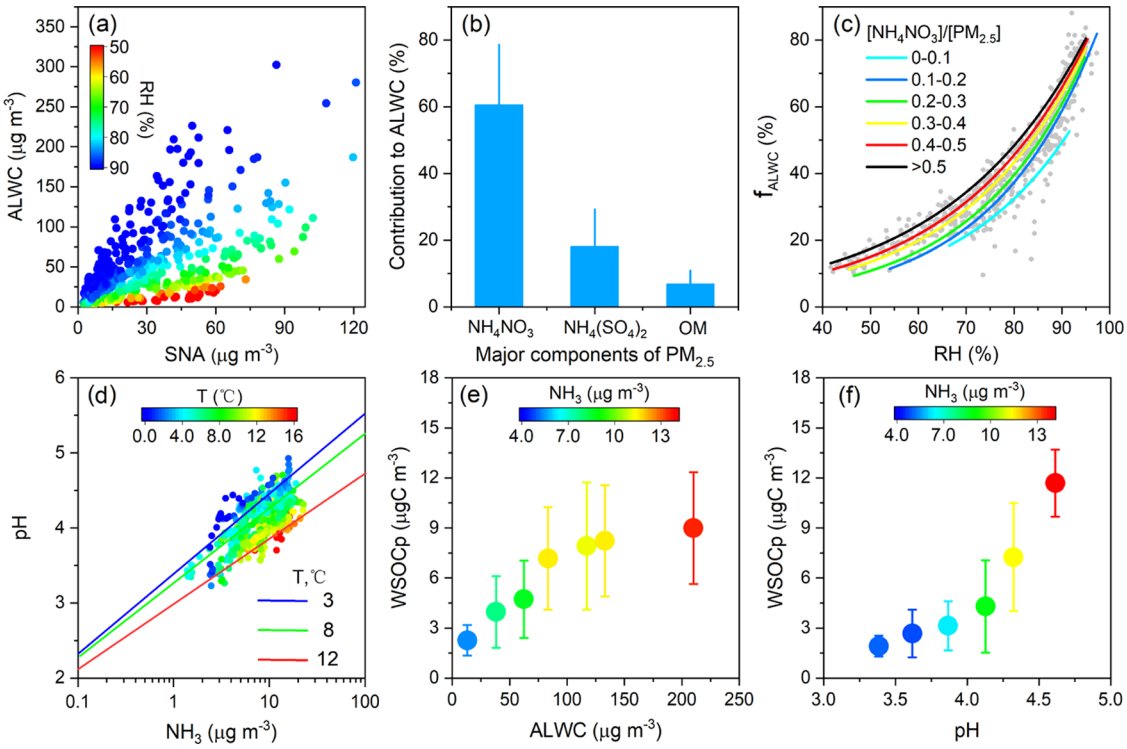

Figure 3. Impacts of ALWC and pH on WSOCg partitioning in the YRD region. (a) Scatter plot of ALWC versus SNA during the whole campaign, (b) average contributions of NH_4NO_3, $(NH_4)_2SO_4$, and OM to ALWC during the whole campaign (calculation details are given in the Supporting Information), (c) relative abundance of ALWC to $PM_{2.5}$ as a function of RH with increasing NH_4NO_3 fractions during the whole campaign, (d) pH dependence of Fp on NH_3 levels under different temperature regimes during the whole campaign, and (e, f) dependence of mass concentrations of WSOCp on ALWC and pH in the high-RH period, respectively.

particle phase. As shown in Table 1, there was a significant difference in Fp between the high- and low-RH periods, especially during the haze episodes (0.47 versus 0.34, respectively, $p < 0.01$), suggesting different partitioning processes under the two RH regimes. The OC concentration in the low-RH period was 60−80% higher than that in the high-RH period and robustly correlated with Fp ($R = 0.70$) in the dry period but not in the humid period (Figure 2a), indicating that the absorbing medium for WSOCg was OM in the relatively dry period. In contrast, a clear increasing trend of Fp along with an increasing ALWC ($R = 0.69$, Figure 2b) was observed during the high-RH phase, indicating that WSOCg in the humid period partitioned into the aerosol aqueous phase, similar to results observed in Atlanta, Los Angeles, and Baltimore in the United States.[34,35]

To further identify the key factors affecting the WSOCg-partitioning process, the correlations of Fp with meteorological conditions (i.e., RH and temperature), aerosol acidity (pH), and NH_3 concentration were analyzed. As shown in Figure S3a, there was no well-defined relationship between Fp and RH in either period ($R \leq 0.3$, $p > 0.05$). In contrast, Fp showed negative correlations with temperature ($R = 0.45$, $p < 0.01$) during the low-RH period (Figure S3b) because WSOCg at high temperature is difficult to convert into the particle phase due to its high volatility, leading to a low partitioning coefficient Fp. The ozone level in the low-RH period (40.0 ± 7.5 $\mu g\ m^{-3}$) was approximately 20% lower than that (49.9 ± 8.4 $\mu g\ m^{-3}$) in the high-RH period, indicating a less active photochemistry in the dry period. Interestingly, we found that the influence of ALWC on WSOCg partitioning during the dry period was insignificant ($R = 0.45$, $p > 0.01$), even at night, when RH was also higher than 80% (Figure S4). As seen in Figure S5a, the condensed phase in the nighttime during the low-RH period was dominated by OM, of which the relative abundance was comparable to that in the daytime but much higher than that in the high-RH period. The abundant OM caused the relative abundance of SNA to OM in the low-RH period to be approximately 3 times lower than that in the high-RH period (Figure S5b). A few studies have found that atmospheric aerosols can exist in a phase-separated format with an organic shell and an inorganic core even at an RH higher than 80%.[36−38] Due to their much weaker water vapor uptake ability compared with SNA, the organic coating can significantly reduce aerosol hygroscopicity, especially when the organic layer is thick. For example, Li et al.[37] investigated the morphology of atmospheric aerosols in the Lesser Khingan Mountains and found that over 59% of the forest particles had an organic shell and did not completely deliquesce until 90% RH. We speculate that the Chongming Island aerosols in the low-RH period were probably phase-separated with an organic shell due to the dominant OM, which significantly reduced the aerosol hygroscopicity and thus resulted in the lower fraction of ALWC when the RH was higher than 80%. Therefore, WSOCg partitioning in the nighttime during the low-RH periods was more significantly affected by the organic phase than by ALW. As seen in Figure S3e−l, compared with ALWC, the pH and NH_3 Fp of both formic and acetic acids in the low-RH period presented a stronger correlation with temperature, further indicating that the partitioning of WSOCg to OM in the low-RH period was a physical condensation process, which dominated the formation pathway of WSOCp.

https://doi.org/10.1021/acs.est.1c06855
Environ. Sci. Technol. 2022, 56, 3915−3924

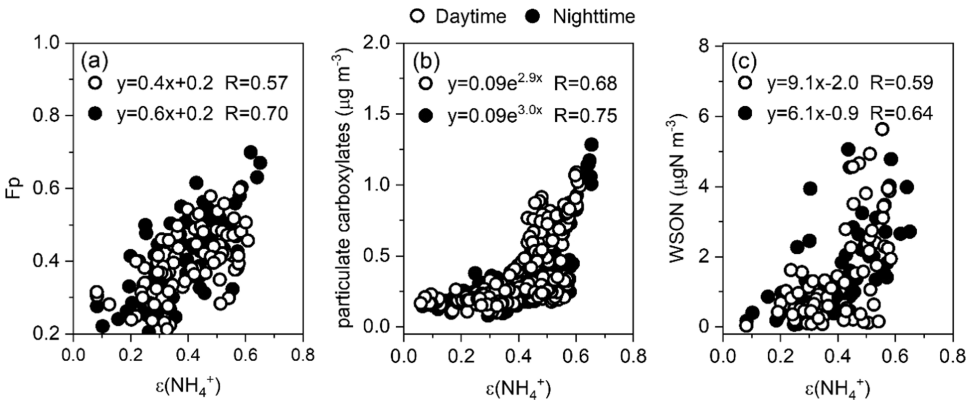

Figure 4. Scatter plots of (a) the partitioning coefficients of WSOC (Fp), (b) carboxylic acids (sum of formic, acetic, and oxalic acids) in $PM_{2.5}$ and (c) water-soluble organic nitrogen (WSON) versus $\varepsilon(NH_4^+)$ of $PM_{2.5}$ in the high-RH period.

3.3. Partitioning of WSOC into the Aerosol Aqueous Phase in the High-RH Period. In this section, we further investigate the effects of ALW, pH, and NH_3 on SOA formation via WSOC aqueous partitioning in the high-RH period since heavy haze events in China mostly occur under humid conditions.[14,17,39] As shown in Figure 3a, ALWC during the campaign increased along with an increase in SNA concentrations, especially under higher-RH conditions. The ISORROPIA-II thermodynamic model calculation results showed that the contribution of NH_4NO_3 to ALWC during the whole campaign period was, on average, 60%, followed by $(NH_4)_2SO_4$ (19%) and OM (6.8%) (Figure 3b). Figure 3c shows that ALWC increased along with an increase in the relative abundance of NH_4NO_3 to $PM_{2.5}$ at a given RH, revealing that ALWC in the YRD region during winter was mainly driven by NH_4NO_3. Furthermore, it can be seen from Figure 3d that pH significantly and positively correlated with NH_3 at a given temperature, suggesting that the ammonia-rich atmosphere in the YRD region is favorable not only for increasing ALWC but also for reducing aerosol acidity, both of which are in turn favorable for WSOCg partitioning, resulting in a clear increasing trend of WSOCp with the enhancements of ALWC and pH (Figure 3e,f).

One explanation for this is that the potential for WSOCg to be partitioned into the aerosol liquid phase is stronger than that into particulate organic matter due to their hydrophilic nature.[40] The pH increased by ammonia actually results in a loss of H^+ from the particle phase and thus further facilitates the ionization equilibrium of acidic organic species to shift into the condensed phase. In contrast to those in the low-RH period, the partitioning coefficients (Fp) of formic and acetic acids during the high-RH period showed a good correlation with ALWC, pH, and NH_3 (Figure S3f−h,j−l). However, the correlations between acetic acid and the three factors were weaker than those for formic acid because formic acid has a higher Henry's law constant.[41] Overall, our results provided strong evidence that during the high-RH period, the enhanced ALWC, pH, and ammonia in the YRD region provided favorable conditions for the partitioning of WSOCg to the aerosol aqueous phase.

In addition to aerosol hygroscopicity and acidity, ammonia also alters WSOCg partitioning through chemical reactions. As shown in Figure 4a, a positively linear correlation between Fp and the NH_3-partitioning coefficient ($\varepsilon(NH_4^+)$), which was defined as the molar ratio between particle ammonia and total ammonia, was found during the high-RH period and was more significant in the nighttime (R = 0.70) than in the daytime (R = 0.57). The results from smog chamber studies by Na et al.[42] and Liu et al.[43] implied that NH_3 could induce a rapid increase in the yields of SOAs from α-pinene ozonolysis and toluene OH radical oxidation, which are attributed to the ammonium salts formed from the neutralization between NH_3 and organic acids. On Chongming Island, exponential growth in particulate carboxylates with an increase in the NH_3-partitioning coefficient ($\varepsilon(NH_4^+)$) was observed during the high-RH period (Figure 4b). The robust correlation between carboxylates and $\varepsilon(NH_4^+)$ observed at both nighttime (R = 0.75) and daytime (R = 0.68) indicated that the neutralization of organic acids with NH_3 to form carboxylates was important under higher-RH conditions. To further elucidate this point, we conducted a thermodynamic calculation on the partitioning behavior of formic and acetic acids (see the details in the SI). As shown in Figure S6, the strong dependences of $\varepsilon(HCOO^-)$ and $\varepsilon(CH_3COO^-)$ on the ambient aerosol acidity in a pH range of 3−5, which were observed at the site and can be well predicted by the S curves with the effective Henry's law constants, clearly demonstrate that the NH_3 neutralization effect was important for the partitioning of WSOCg into the aerosol phase in the high-RH period.

Another reaction between ammonia and WSOC in the particle phase is the aqueous-phase reaction of ammonia with carbonyl species. Laboratory studies have shown that the uptake of ammonia by carbonyl groups in the aqueous phase can form nitrogen-containing organic compounds via the Maillard reaction.[44,45] As shown in Figure 4c, there was a positive correlation between WSON and $\varepsilon(NH_4^+)$ on Chongming Island during the high-RH period. Previous studies have shown that most of the WSON produced from the Maillard reaction is light-absorbing brown carbon (BrC).[46] Indeed, in this study, the light absorption of WSOCp in a wavelength range of 300−550 nm during the high-RH period significantly increased with increasing WSON and $\varepsilon(NH_4^+)$ (Figure S7), indicating BrC formation in the humid period, especially in the heavy haze period. Such a reaction can result in the loss of free carbonyls in the aqueous phase, and thus gaseous carbonyls must partition into the aqueous phase to maintain equilibrium, leading to a higher Fp. Moreover, the enhanced WSOCp formation can also be facilitated by a carbenium ion-mediated mechanism related to dicarbonyls.[47] Generally, such a positive correlation of WSON with $\varepsilon(NH_4^+)$ suggested that a high concentration of ammonia under humid conditions enhanced WSOCg partitioning not only by

https://doi.org/10.1021/acs.est.1c06855
Environ. Sci. Technol. 2022, 56, 3915−3924

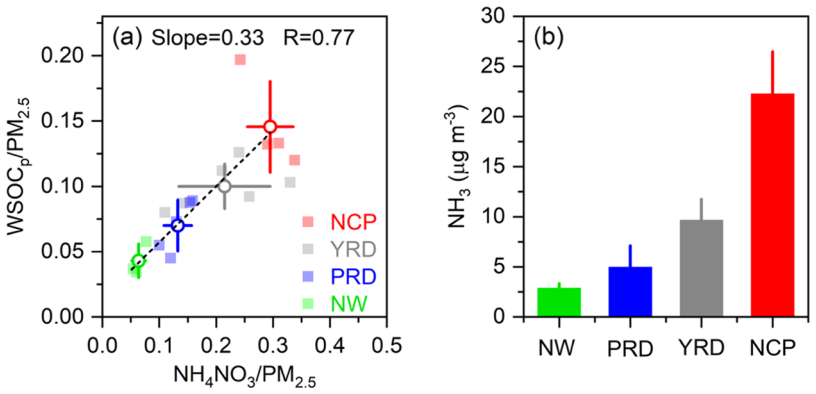

Figure 5. Impact of NH_3 on WSOCp distribution in different regions of China. (a) WSOCp mass fractions as a function of NH_4NO_3 mass fractions and (b) NH_3 concentrations (Data except for this study are reanalyzed from the literature. Detailed information on the specific sites, time periods, and sources of the datasets is given in Tables S1 and S2.).

increasing ALWC and pH but also by promoting aerosol aqueous reactions, which can remarkably promote SOA formation.

3.4. Effect of NH_3 on the Spatial Distribution of SOAs in China. To further explore the impact of NH_3 on WSOC partitioning in the country, the relationship between the mass ratio of WSOCp to $PM_{2.5}$ and that of NH_4NO_3 to $PM_{2.5}$ and the spatial distribution of NH_3 concentration in different regions of China were statistically explored on a national scale (Figure 5 and Tables S1 and S2). As seen in Figure 5a, a robust linear correlation (R = 0.77) was found between the mass ratio of WSOCp to $PM_{2.5}$ and that of NH_4NO_3 to $PM_{2.5}$. However, such a correlation was not observed for sulfate (Figure S8) because gas-aerosol phase partitioning is the dominant formation pathway for both WSOCp and NH_4NO_3, while sulfate is largely formed in aqueous phases such as wetted aerosols, fog, and cloud droplets.[17,19] Although the absolute concentration varied due to the differences in emissions and weather conditions in different regions in different years, both NH_4NO_3 and WSOCp fractions in $PM_{2.5}$ were found to be the highest on the North China Plain (NCP), followed by those in the YRD and Pearl River Delta (PRD) regions (Figure 5a). The lowest fractions appeared in Lanzhou and Qinghai Lake, both of which are located in Northwest (NW) China. Such a spatial distribution is in accordance with the concentration of NH_3 (Figure 5b). As shown in Tables S1 and S2, NH_3 emissions on the NCP are the highest in China due to intensive agricultural activities[48,49] and are the lowest in Northwest (NW) China due to the sparse population and much lower fertilizer usage.[49] Such a coincident spatial pattern suggests that the ammonia-rich conditions in China provide a favorable environment for WSOCg partitioning at a national scale and thus may enhance SOA production.

4. IMPLICATIONS FOR ATMOSPHERIC CHEMISTRY

The national burden of NH_3 has been serious in the past decade and even increasing as China has not promulgated specific policies toward NH_3 emission control.[49] The ammonia-rich atmosphere in China, together with the effective sulfur emission control, has resulted in a higher mass fraction of nitrate than sulfate due to the reduced competition for ammonium.[14,50] Such a change in atmospheric aerosol compositions can enhance ALW formation since nitrate is more hygroscopic than sulfate at a given RH and aerosol loading.[51] Previous studies reported that an elevation in ALW driven by nitrate may speed up the uptake of inorganic fractions, leading to a positive feedback loop.[16,52,53] However, our work here demonstrates for the first time that this feedback loop also tends to promote the partitioning of WSOCg and thus can enhance SOA formation.

As the major alkaline gas in the atmosphere, NH_3 not only regulates aerosol acidity through neutralization with acidic compounds but also participates in the formation of SOA. Our recent chamber simulation found that NH_3 has a synergetic effect with NO_x on SOA formation from toluene photooxidation and the optical adsorption of secondary products by forming N-containing organic aerosols.[43,54] Such a synergetic process is dominated by aqueous-phase reactions and is thus more significant under high-RH conditions. In this study, we found that compared with that in the United States and other countries, the larger yield of WSOCp in China can be attributed to an enhanced uptake of WSOCg by ALWC that is driven by NH_4NO_3 and aqueous-phase reactions such as acid−base neutralization due to the abundant NH_3, which can result in less WSOCp partitioning into the gas phase and can thus efficiently increase the SOA yield.[44,45,55] Since SOA and NH_4NO_3 account for a major part of $PM_{2.5}$ in the country, especially in haze periods,[11,14,50] our work suggests that emission control of NH_3 is indispensable for air pollution mitigation, especially SOAs in China.

■ ASSOCIATED CONTENT

Supporting Information

The Supporting Information is available free of charge at https://pubs.acs.org/doi/10.1021/acs.est.1c06855.

Additional details of the online measurements by the IGAC, calculation of the ALWC contribution, and concentrations of NH_3 and WSOC and SNA of $PM_{2.5}$ from different regions of China (PDF)

■ AUTHOR INFORMATION

Corresponding Author

Gehui Wang − *Key Lab of Geographic Information Science of the Ministry of Education, School of Geographic Sciences, East China Normal University, Shanghai 200062, China; Institute of Eco-Chongming, Shanghai 202162, China;* orcid.org/0000-0002-0181-4685; Email: ghwang@geo.ecnu.edu.cn

https://doi.org/10.1021/acs.est.1c06855
Environ. Sci. Technol. 2022, 56, 3915−3924

Authors

Shaojun Lv − *Key Lab of Geographic Information Science of the Ministry of Education, School of Geographic Sciences, East China Normal University, Shanghai 200062, China*

Fanglin Wang − *Key Lab of Geographic Information Science of the Ministry of Education, School of Geographic Sciences, East China Normal University, Shanghai 200062, China*

Can Wu − *Key Lab of Geographic Information Science of the Ministry of Education, School of Geographic Sciences, East China Normal University, Shanghai 200062, China;* orcid.org/0000-0003-2025-2646

Yubao Chen − *Key Lab of Geographic Information Science of the Ministry of Education, School of Geographic Sciences, East China Normal University, Shanghai 200062, China*

Shijie Liu − *Key Lab of Geographic Information Science of the Ministry of Education, School of Geographic Sciences, East China Normal University, Shanghai 200062, China*

Si Zhang − *Key Lab of Geographic Information Science of the Ministry of Education, School of Geographic Sciences, East China Normal University, Shanghai 200062, China*

Dapeng Li − *Key Lab of Geographic Information Science of the Ministry of Education, School of Geographic Sciences, East China Normal University, Shanghai 200062, China*

Wei Du − *Key Lab of Geographic Information Science of the Ministry of Education, School of Geographic Sciences, East China Normal University, Shanghai 200062, China*

Fan Zhang − *Key Lab of Geographic Information Science of the Ministry of Education, School of Geographic Sciences, East China Normal University, Shanghai 200062, China*

Hongli Wang − *State Environmental Protection Key Laboratory of Cause and Prevention of Urban Air Pollution Complex, Shanghai Academy of Environmental Sciences, Shanghai 200233, China;* orcid.org/0000-0003-0655-3389

Cheng Huang − *State Environmental Protection Key Laboratory of Cause and Prevention of Urban Air Pollution Complex, Shanghai Academy of Environmental Sciences, Shanghai 200233, China;* orcid.org/0000-0001-9518-3628

Qingyan Fu − *Shanghai Environmental Monitoring Center, Shanghai 200232, China*

Yusen Duan − *Shanghai Environmental Monitoring Center, Shanghai 200232, China*

Complete contact information is available at: https://pubs.acs.org/10.1021/acs.est.1c06855

Author Contributions

G.W. designed the research. S.L. and F.W. conducted the experiment. Y.C., C.W., W.D., S.L., S.Z., and D.L. performed the $PM_{2.5}$ sampling. S.L. and G.W. analyzed the data and wrote the paper. Other authors contributed to this work with helpful discussions.

Notes

The authors declare no competing financial interest.

■ ACKNOWLEDGMENTS

This work was funded by the National Natural Science Foundation of China (nos. 41773117, 42007202, and 42130704), the programs from Shanghai Science and Technology Innovation Action Plan (20dz1204011), and Institute of Eco-Chongming and ECNU Happiness Flower.

■ REFERENCES

(1) Satish, R.; Shamjad, P.; Thamban, N.; Tripathi, S.; Rastogi, N. Temporal characteristics of brown carbon over the central Indo-Gangetic Plain. *Environ. Sci. Technol.* **2017**, *51*, 6765−6772.

(2) Jimenez, J. L.; Canagaratna, M. R.; Donahue, N. M.; Prevot, A. S. H.; Zhang, Q.; Kroll, J. H.; DeCarlo, P. F.; Allan, J. D.; Coe, H.; Ng, N. L.; Aiken, A. C.; Docherty, K. S.; Ulbrich, I. M.; Grieshop, A. P.; Robinson, A. L.; Duplissy, J.; Smith, J. D.; Wilson, K. R.; Lanz, V. A.; Hueglin, C.; Sun, Y. L.; Tian, J.; Laaksonen, A.; Raatikainen, T.; Rautiainen, J.; Vaattovaara, P.; Ehn, M.; Kulmala, M.; Tomlinson, J. M.; Collins, D. R.; Cubison, M. J.; Dunlea, E. J.; Huffman, J. A.; Onasch, T. B.; Alfarra, M. R.; Williams, P. I.; Bower, K.; Kondo, Y.; Schneider, J.; Drewnick, F.; Borrmann, S.; Weimer, S.; Demerjian, K.; Salcedo, D.; Cottrell, L.; Griffin, R.; Takami, A.; Miyoshi, T.; Hatakeyama, S.; Shimono, A.; Sun, J. Y.; Zhang, Y. M.; Dzepina, K.; Kimmel, J. R.; Sueper, D.; Jayne, J. T.; Herndon, S. C.; Trimborn, A. M.; Williams, L. R.; Wood, E. C.; Middlebrook, A. M.; Kolb, C. E.; Baltensperger, U.; Worsnop, D. R. Evolution of Organic Aerosols in the Atmosphere. *Science* **2009**, *326*, 1525−1529.

(3) Zhao, C.; Niu, M.; Song, S.; Li, J.; Su, Z.; Wang, Y.; Gao, Q.; Wang, H. Serum metabolomics analysis of mice that received repeated airway exposure to a water-soluble PM2.5 extract. *Ecotoxicol. Environ. Saf.* **2019**, *168*, 102−109.

(4) Wen, J.; Shi, G.; Tian, Y.; Chen, G.; Liu, J.; Huang-Fu, Y.; Ivey, C. E.; Feng, Y. Source contributions to water-soluble organic carbon and water-insoluble organic carbon in PM2.5 during Spring Festival, heating and non-heating seasons. *Ecotoxicol. Environ. Saf.* **2018**, *164*, 172−180.

(5) Ding, X.; He, Q.-F.; Shen, R.-Q.; Yu, Q.-Q.; Wang, X.-M. Spatial distributions of secondary organic aerosols from isoprene, monoterpenes, beta-caryophyllene, and aromatics over China during summer. *J. Geophys. Res.: Atmos.* **2014**, *119*, 11877−11891.

(6) Lv, S.; Gong, D.; Ding, Y.; Lin, Y.; Wang, H.; Ding, H.; Wu, G.; He, C.; Zhou, L.; Liu, S.; Ristovski, Z.; Chen, D.; Shao, M.; Zhang, Y.; Wang, B. Elevated levels of glyoxal and methylglyoxal at a remote mountain site in southern China: Prompt in-situ formation combined with strong regional transport. *Sci. Total Environ.* **2019**, *672*, 869−882.

(7) Shen, G.; Tao, S.; Wei, S.; Chen, Y.; Zhang, Y.; Shen, H.; Huang, Y.; Zhu, D.; Yuan, C.; Wang, H.; Wang, Y.; Pei, L.; Liao, Y.; Duan, Y.; Wang, B.; Wang, R.; Lv, Y.; Li, W.; Wang, X.; Zheng, X. Field Measurement of Emission Factors of PM, EC, OC, Parent, Nitro-, and Oxy- Polycyclic Aromatic Hydrocarbons for Residential Briquette, Coal Cake, and Wood in Rural Shanxi, China. *Environ. Sci. Technol.* **2013**, *47*, 2998−3005.

(8) Ervens, B.; Turpin, B. J.; Weber, R. J. Secondary organic aerosol formation in cloud droplets and aqueous particles (aqSOA): a review of laboratory, field and model studies. *Atmos. Chem. Phys.* **2011**, *11*, 11069−11102.

(9) McNeill, V. F. Aqueous organic chemistry in the atmosphere: Sources and chemical Processing of Organic Aerosols. *Environ. Sci. Technol.* **2015**, *49*, 1237−1244.

(10) Shen, H.; Chen, Z.; Li, H.; Qian, X.; Qin, X.; Shi, W. Gas-Particle Partitioning of Carbonyl Compounds in the Ambient Atmosphere. *Environ. Sci. Technol.* **2018**, *52*, 10997−11006.

(11) Zhang, R.; Wang, G.; Guo, S.; Zamora, M. L.; Ying, Q.; Lin, Y.; Wang, W.; Hu, M.; Wang, Y. Formation of urban fine particulate matter. *Chem. Rev.* **2015**, *115*, 3803−3855.

(12) Hennigan, C. J.; Bergin, M. H.; Russell, A. G.; Nenes, A.; Weber, R. J. Gas/particle partitioning of water-soluble organic aerosol in Atlanta. *Atmos. Chem. Phys.* **2009**, *9*, 3613−3628.

(13) Nah, T.; Guo, H. Y.; Sullivan, A. P.; Chen, Y. L.; Tanner, D. J.; Nenes, A.; Russell, A.; Ng, N. L.; Huey, L. G.; Weber, R. J. Characterization of aerosol composition, aerosol acidity, and organic acid partitioning at an agriculturally intensive rural southeastern US site. *Atmos. Chem. Phys.* **2018**, *18*, 11471−11491.

(14) Xie, Y. N.; Wang, G. H.; Wang, X. P.; Chen, J. M.; Chen, Y. B.; Tang, G. Q.; Wang, L. L.; Ge, S. S.; Xue, G. Y.; Wang, Y. S.; Gao, J. Nitrate-dominated $PM_{2.5}$ and elevation of particle pH observed in

urban Beijing during the winter of 2017. *Atmos. Chem. Phys.* **2020**, *20*, 5019−5033.
(15) Hodas, N.; Sullivan, A. P.; Skog, K.; Keutsch, F. N.; Collett, J. L.; Decesari, S.; Facchini, M. C.; Carlton, A. G.; Laaksonen, A.; Turpin, B. J. Aerosol Liquid Water Driven by Anthropogenic Nitrate: Implications for Lifetimes of Water-Soluble Organic Gases and Potential for Secondary Organic Aerosol Formation. *Environ. Sci. Technol.* **2014**, *48*, 11127−11136.
(16) Ge, B. Z.; Xu, X. B.; Ma, Z. Q.; Pan, X. L.; Wang, Z.; Lin, W. L.; Ouyang, B.; Xu, D. H.; Lee, J.; Zheng, M.; Ji, D. S.; Sun, Y. L.; Dong, H. B.; Squires, F. A.; Fu, P. Q.; Wang, Z. F. Role of Ammonia on the Feedback Between AWC and Inorganic Aerosol Formation During Heavy Pollution in the North China Plain. *Earth Space Sci.* **2019**, *6*, 1675−1693.
(17) Wang, G.; Zhang, R.; Gomez, M. E.; Yang, L.; Zamora, M. L.; Hu, M.; Lin, Y.; Peng, J.; Guo, S.; Meng, J.; Li, J.; Cheng, C.; Hu, T.; Ren, Y.; Wang, Y.; Gao, J.; Cao, J.; An, Z.; Zhou, W.; Li, G.; Wang, J.; Tian, P.; Marrero-Ortiz, W.; Secrest, J.; Du, Z.; Zheng, J.; Shang, D.; Zeng, L.; Shao, M.; Wang, W.; Huang, Y.; Wang, Y.; Zhu, Y.; Li, Y.; Hu, J.; Pan, B.; Cai, L.; Cheng, Y.; Ji, Y.; Zhang, F.; Rosenfeld, D.; Liss, P. S.; Duce, R. A.; Kolb, C. E.; Molina, M. J. Persistent sulfate formation from London Fog to Chinese haze. *Proc. Natl. Acad. Sci. U.S.A.* **2016**, *113*, 13630−13635.
(18) Pye, H. O. T.; Murphy, B. N.; Xu, L.; Ng, N. L.; Carlton, A. G.; Guo, H. Y.; Weber, R.; Vasilakos, P.; Appel, K. W.; Budisulistiorini, S. H.; Surratt, J. D.; Nenes, A.; Hu, W. W.; Jimenez, J. L.; Isaacman-VanWertz, G.; Misztal, P. K.; Goldstein, A. H. On the implications of aerosol liquid water and phase separation for organic aerosol mass. *Atmos. Chem. Phys.* **2017**, *17*, 343−369.
(19) Wang, G.; Zhang, F.; Peng, J.; Duan, L.; Ji, Y.; Marrero-Ortiz, W.; Wang, J.; Li, J.; Wu, C.; Cao, C.; Wang, Y.; Zheng, J.; Secrest, J.; Li, Y.; Wang, Y.; Li, H.; Li, N.; Zhang, R. Particle acidity and sulfate production during severe haze events in China cannot be reliably inferred by assuming a mixture of inorganic salts. *Atmos. Chem. Phys.* **2018**, *18*, 10123−10132.
(20) Wu, C.; Wang, G. H.; Li, J.; Li, J. J.; Cao, C.; Ge, S. S.; Xie, Y. N.; Chen, J. M.; Liu, S. J.; Du, W.; Zhao, Z. Y.; Cao, F. Non-agricultural sources dominate the atmospheric NH3 in Xi'an, a megacity in the semi-arid region of China. *Sci. Total Environ.* **2020**, *722*, No. 137756.
(21) Xu, J.; Chen, J.; Shi, Y.; Zhao, N.; Qin, X.; Yu, G.; Liu, J.; Lin, Y.; Fu, Q.; Weber, R. J.; Lee, S.-H.; Deng, C.; Huang, K. First Continuous Measurement of Gaseous and Particulate Formic Acid in a Suburban Area of East China: Seasonality and Gas-Particle Partitioning. *ACS Earth Space Chem.* **2020**, *4*, 157−167.
(22) Cui, Jn.; Sun, M.; Wang, L.; Guo, J.; Xie, G.; Zhang, J.; Zhang, R. Gas-particle partitioning of carbonyls and its influencing factors in the urban atmosphere of Zhengzhou, China. *Sci. Total Environ.* **2021**, *751*, No. 142027.
(23) Wang, G. H.; Zhou, B. H.; Cheng, C. L.; Cao, J. J.; Li, J. J.; Meng, J. J.; Tao, J.; Zhang, R. J.; Fu, P. Q. Impact of Gobi desert dust on aerosol chemistry of Xi'an, inland China during spring 2009: differences in composition and size distribution between the urban ground surface and the mountain atmosphere. *Atmos. Chem. Phys.* **2013**, *13*, 819−835.
(24) Wu, C.; Wang, G. H.; Li, J.; Li, J. J.; Cao, C.; Ge, S. S.; Xie, Y. N.; Chen, J. M.; Li, X. R.; Xue, G. Y.; Wang, X. P.; Zhao, Z. Y.; Cao, F. The characteristics of atmospheric brown carbon in Xi'an, inland China: sources, size distributions and optical properties. *Atmos. Chem. Phys.* **2020**, *20*, 2017−2030.
(25) Ge, X. L.; Shaw, S. L.; Zhang, Q. Toward Understanding Amines and Their Degradation Products from Postcombustion CO2 Capture Processes with Aerosol Mass Spectrometry. *Environ. Sci. Technol.* **2014**, *48*, 5066−5075.
(26) He, Y. X.; Pan, Y. P.; Zhang, G. Z.; Ji, D. S.; Tian, S. L.; Xu, X. J.; Zhang, R. J.; Wang, Y. S. Tracking ammonia morning peak, sources and transport with 1 Hz measurements at a rural site in North China Plain. *Atmos. Environ.* **2020**, *235*, No. 117630.
(27) Wu, C.; Wang, G.; Li, J.; Li, J.; Cao, C.; Ge, S.; Xie, Y.; Chen, J.; Li, X.; Xue, G.; Wang, X.; Zhao, Z.; Cao, F. The characteristics of atmospheric brown carbon in Xi'an, inland China: sources, size distributions and optical properties. *Atmos. Chem. Phys.* **2020**, *20*, 2017−2030.
(28) Fountoukis, C.; Nenes, A. ISORROPIA II: a computationally efficient thermodynamic equilibrium model for K^+-Ca^{2+}-Mg^{2+}-NH_4^+-Na^+-SO_4^{2-}-NO_3^--Cl^--H_2O aerosols. *Atmos. Chem. Phys.* **2007**, *7*, 4639−4659.
(29) Hennigan, C. J.; Izumi, J.; Sullivan, A. P.; Weber, R. J.; Nenes, A. A critical evaluation of proxy methods used to estimate the acidity of atmospheric particles. *Atmos. Chem. Phys.* **2015**, *15*, 2775−2790.
(30) Guo, H.; Xu, L.; Bougiatioti, A.; Cerully, K. M.; Capps, S. L.; Hite, J. R.; Carlton, A. G.; Lee, S. H.; Bergin, M. H.; Ng, N. L.; Nenes, A.; Weber, R. J. Fine-particle water and pH in the southeastern United States. *Atmos. Chem. Phys.* **2015**, *15*, 5211−5228.
(31) Gong, L. W.; Lewicki, R.; Griffin, R. J.; Tittel, F. K.; Lonsdale, C. R.; Stevens, R. G.; Pierce, J. R.; Malloy, Q. G. J.; Travis, S. A.; Bobmanuel, L. M.; Lefer, B. L.; Flynn, J. H. Role of atmospheric ammonia in particulate matter formation in Houston during summertime. *Atmos. Environ.* **2013**, *77*, 893−900.
(32) Li, Y.; Schwandner, F. M.; Sewell, H. J.; Zivkovich, A.; Tigges, M.; Raja, S.; Holcomb, S.; Molenar, J. V.; Sherman, L.; Archuleta, C.; Lee, T.; Collett, J. L. Observations of ammonia, nitric acid, and fine particles in a rural gas production region. *Atmos. Environ.* **2014**, *83*, 80−89.
(33) Renbaum-Wolff, L.; Grayson, J. W.; Bateman, A. P.; Kuwata, M.; Sellier, M.; Murray, B. J.; Shilling, J. E.; Martin, S. T.; Bertram, A. K. Viscosity of alpha-pinene secondary organic material and implications for particle growth and reactivity. *Proc. Natl. Acad. Sci. U.S.A.* **2013**, *110*, 8014−8019.
(34) Zhang, X. L.; Liu, J. M.; Parker, E. T.; Hayes, P. L.; Jimenez, J. L.; de Gouw, J. A.; Flynn, J. H.; Grossberg, N.; Lefer, B. L.; Weber, R. J. On the gas-particle partitioning of soluble organic aerosol in two urban atmospheres with contrasting emissions: 1. Bulk water-soluble organic carbon. *J. Geophys. Res.: Atmos.* **2012**, *117*, No. D00V16.
(35) El-Sayed, M. M. H.; Ortiz-Montalvo, D. L.; Hennigan, C. J. The effects of isoprene and NOx on secondary organic aerosols formed through reversible and irreversible uptake to aerosol water. *Atmos. Chem. Phys.* **2018**, *18*, 1171−1184.
(36) Yu, H.; Li, W. J.; Zhang, Y. M.; Tunved, P.; Dall'Osto, M.; Shen, X. J.; Sun, J. Y.; Zhang, X. Y.; Zhang, J. C.; Shi, Z. B. Organic coating on sulfate and soot particles during late summer in the Svalbard Archipelago. *Atmos. Chem. Phys.* **2019**, *19*, 10433−10446.
(37) Li, W. J.; Teng, X. M.; Chen, X. Y.; Liu, L.; Xu, L.; Zhang, J.; Wang, Y. Y.; Zhang, Y.; Shi, Z. B. Organic Coating Reduces Hygroscopic Growth of Phase-Separated Aerosol Particles. *Environ. Sci. Technol.* **2021**, *55*, 16339−16346.
(38) Ushijima, S. B.; Huynh, E.; Davis, R. D.; Tolbert, M. A. Seeded Crystal Growth of Internally Mixed Organic-Inorganic Aerosols: Impact of Organic Phase State. *J. Phys. Chem. A* **2021**, *125*, 8668−8679.
(39) Ge, S. S.; Wang, G. H.; Zhang, S.; Li, D. P.; Xie, Y. N.; Wu, C.; Yuan, Q.; Chen, J. M.; Zhang, H. L. Abundant NH3 in China Enhances Atmospheric HONO Production by Promoting the Heterogeneous Reaction of SO_2 with NO_2. *Environ. Sci. Technol.* **2019**, *53*, 14339−14347.
(40) Carlton, A. G.; Turpin, B. J. Particle partitioning potential of organic compounds is highest in the Eastern US and driven by anthropogenic water. *Atmos. Chem. Phys.* **2013**, *13*, 10203−10214.
(41) Sander, R. Compilation of Henry's law constants (version 4.0) for water as solvent. *Atmos. Chem. Phys.* **2015**, *15*, 4399−4981.
(42) Na, K.; Song, C.; Switzer, C.; Cocker, D. R., III Effect of ammonia on secondary organic aerosol formation from alpha-Pinene ozonolysis in dry and humid conditions. *Environ. Sci. Technol.* **2007**, *41*, 6096−6102.
(43) Liu, S. J.; Huang, D. D.; Wang, Y. Q.; Zhang, S.; Liu, X. D.; Wu, C.; Du, W.; Wang, G. H. Synergetic effects of NH_3 and NO_X on the production and optical absorption of secondary organic aerosol

https://doi.org/10.1021/acs.est.1c06855
Environ. Sci. Technol. 2022, 56, 3915−3924

formation from toluene photooxidation. *Atmos. Chem. Phys.* **2021**, *21*, 17759−17773.
(44) Li, Y.; Zhao, J.; Wang, Y.; Seinfeld, J. H.; Zhang, R. Multigeneration Production of Secondary Organic Aerosol from Toluene Photooxidation. *Environ. Sci. Technol.* **2021**, *55*, 8592−8603.
(45) Li, Y.; Ji, Y.; Zhao, J.; Wang, Y.; Shi, Q.; Peng, J.; Wang, Y.; Wang, C.; Zhang, F.; Wang, Y.; Seinfeld, J. H.; Zhang, R. Unexpected Oligomerization of Small alpha-Dicarbonyls for Secondary Organic Aerosol and Brown Carbon Formation. *Environ. Sci. Technol.* **2021**, *55*, 4430−4439.
(46) Laskin, A.; Laskin, J.; Nizkorodov, S. A. Chemistry of Atmospheric Brown Carbon. *Chem. Rev.* **2015**, *115*, 4335−4382.
(47) Ji, Y.; Shi, Q.; Li, Y.; An, T.; Zheng, J.; Peng, J.; Gao, Y.; Chen, J.; Li, G.; Wang, Y.; Zhang, F.; Zhang, A. L.; Zhao, J.; Molina, M. J.; Zhang, R. Carbenium ion-mediated oligomerization of methylglyoxal for secondary organic aerosol formation. *Proc. Natl. Acad. Sci. U.S.A.* **2020**, *117*, 13294−13299.
(48) Pan, Y. P.; Tian, S. L.; Zhao, Y. H.; Zhang, L.; Zhu, X. Y.; Gao, J.; Huang, W.; Zhou, Y. B.; Song, Y.; Zhang, Q.; Wang, Y. S. Identifying Ammonia Hotspots in China Using a National Observation Network. *Environ. Sci. Technol.* **2018**, *52*, 3926−3934.
(49) Chen, S. H.; Cheng, M. M.; Guo, Z.; Xu, W.; Du, X. H.; Li, Y. Enhanced atmospheric ammonia (NH_3) pollution in China from 2008 to 2016: Evidence from a combination of observations and emissions. *Environ. Pollut.* **2020**, *263*, No. 114421.
(50) Bellouin, N.; Rae, J.; Jones, A.; Johnson, C.; Haywood, J.; Boucher, O. Aerosol forcing in the Climate Model Intercomparison Project (CMIP5) simulations by HadGEM2-ES and the role of ammonium nitrate. *J. Geophys. Res.: Atmos.* **2011**, *116*, No. D20206.
(51) Bai, Z. P.; Ji, Y.; Pi, Y. Q.; Yang, K. X.; Wang, L.; Zhang, Y. Q.; Zhai, Y. D.; Yan, Z. G.; Han, X. D. Hygroscopic analysis of individual Beijing haze aerosol particles by environmental scanning electron microscopy. *Atmos. Environ.* **2018**, *172*, 149−156.
(52) Wu, Z.; Wang, Y.; Tan, T.; Zhu, Y.; Li, M.; Shang, D.; Wang, H.; Lu, K.; Guo, S.; Zeng, L.; Zhang, Y. Aerosol Liquid Water Driven by Anthropogenic Inorganic Salts: Implying Its Key Role in Haze Formation over the North China Plain. *Environ. Sci. Technol. Lett.* **2018**, *5*, 160−166.
(53) Peng, J. F.; Hu, M.; Shang, D. J.; Wu, Z. J.; Du, Z. F.; Tan, T. Y.; Wang, Y. N.; Zhang, F.; Zhang, R. Y. Explosive Secondary Aerosol Formation during Severe Haze in the North China Plain. *Environ. Sci. Technol.* **2021**, *55*, 2189−2207.
(54) Marrero-Ortiz, W.; Hu, M.; Du, Z. F.; Ji, Y. M.; Wang, Y. J.; Guo, S.; Lin, Y.; Gomez-Hermandez, M.; Peng, J. F.; Li, Y. X.; Secrest, J.; Zamora, M. L.; Wang, Y.; An, T. C.; Zhang, R. Y. Formation and Optical Properties of Brown Carbon from Small alpha-Dicarbonyls and Amines. *Environ. Sci. Technol.* **2019**, *53*, 117−126.
(55) Liu, S.; Huang, D.; Wang, Y.; Zhang, S.; Liu, X.; Wu, C.; Du, W.; Wang, G. Synergetic effects of NH_3 and NOx on the production and optical absorption of secondary organic aerosol formation from toluene photooxidation. *Atmos. Chem. Phys.* **2021**, *21*, 17759−17773.

https://doi.org/10.1021/acs.est.1c06855
Environ. Sci. Technol. 2022, 56, 3915−3924